

Six-Dimensional Simulations of Core-Collapse Supernovae with Full Boltzmann Neutrino Transport

Hiroki Nagakura¹, Wakana Iwakami^{2,3}, Shun Furusawa⁴, Hirotada Okawa^{2,3}, Akira Harada⁵,
Kohsuke Sumiyoshi⁶, Shoichi Yamada^{3,7}, Hideo Matsufuru⁸ and Akira Imakura⁹

¹*TAPIR, Walter Burke Institute for Theoretical Physics, Mailcode 350-17,
California Institute of Technology, Pasadena, CA 91125, USA*

²*Yukawa Institute for Theoretical Physics, Kyoto University,
Oiwake-cho, Kitashirakawa, Sakyo-ku, Kyoto, 606-8502, Japan*

³*Advanced Research Institute for Science & Engineering,
Waseda University, 3-4-1 Okubo, Shinjuku, Tokyo 169-8555, Japan*

⁴*Frankfurt Institute for Advanced Studies, J.W.Goethe University, D-60438 Frankfurt am Main, Germany*

⁵*Department of Physics, University of Tokyo, 7-3-1 Hongo, Bunkyo, Tokyo 113-0033, Japan*

⁶*Numazu College of Technology, Ooka 3600, Numazu, Shizuoka 410-8501, Japan*

⁷*Department of Science and Engineering, Waseda University, 3-4-1 Okubo, Shinjuku, Tokyo 169-8555, Japan*

⁸*High Energy Accelerator Research Organization, 1-1 Oho, Tsukuba, Ibaraki 308-0801, Japan and*

⁹*University of Tsukuba, 1-1-1, Tennodai Tsukuba, Ibaraki 305-8577, Japan*

This is the first-ever report of much awaited core-collapse supernova simulations with solving the Boltzmann equations for neutrino transport, which actually amounts to a 6-dimensional (1 in time, 2 in space and 3 in momentum space) problem even under axial symmetry. This is also the first study to find a sign of successful explosion in a computation at this level of elaboration in neutrino transport. We also investigate the neutrino distributions in momentum space, which would not be accessible to other approximate methods employed so far. The off-diagonal component of the Eddington tensor for neutrinos derived in this letter is different from what are prescribed by hand in frequently-used approximations. The results will be useful to test and possibly improve these approximations casually used but not validated in the literature.

PACS numbers:

Introduction.— The theoretical study of the explosion mechanism of core-collapse supernovae (CCSNe) has heavily relied on numerical simulations. This is mainly because CCSNe are rare: it occurs a few times in a century per galaxy on average [1–7] and, in fact, SN1987A is the only one close enough to extract some useful information on what happened deep inside the massive star from, among other things, the detection of neutrinos [8, 9]. Since the CCSNe are intrinsically multi-scale, multi-physics and multi-dimensional (multi-D) phenomena, their mechanism can be addressed only with detailed numerical computations. Although the recent progress is remarkable indeed, even the most sophisticated multi-D simulations of CCSNe done so far employed approximations one way or another in their numerical treatment of neutrino transport [10–26]. That may be crucial to their outcomes, since some of these calculations, which adopted different approximations, seem to be at odds with each other. The best way to calibrate them should obviously be to compare them with what is obtained without appealing to those artificial approximations, i.e., the results of first-principles simulations just like what happened for spherically symmetric computations more than a decade ago [27–29].

In axisymmetry, this is possible now and we achieved such simulations with the K supercomputer in Japan, one of the currently available best supercomputers with ~ 10 PFLOPS. In this study we discretized the Boltzmann equations both in space and momentum, which

is actually a 6-dimensional problem even under axisymmetry. Except for this almost mandatory discretization of the basic differential equations, we do not resort to any artificial approximation or phenomenological modeling in the neutrino transport [32, 33]. Note that Ott et al. [10] also conducted axisymmetric simulations, discretizing the Boltzmann equations, but they took in fact a hybrid approach that employed the multi-group flux-limited diffusion approximation in the optically thick region, i.e., theirs were not genuinely the full Boltzmann-neutrino transport. More importantly, they ignored relativistic corrections completely, dropping all fluid-velocity dependent terms, and also neglected some important neutrino-matter reactions, all of which are crucial for realistic modeling of CCSNe (see e.g., [30, 31]).

These days, much attention of supernova researchers is directed to 3-dimensional simulations in space. It should be remembered, however, that those computations inevitably employ some approximations in neutrino transport, which have not been well validated even in axisymmetry. We believe that the results presented here are not only a milestone for the numerical study of CCSNe, but they are also important as realistic supernova models, albeit in axisymmetry. They will hopefully contribute to the resolution of the apparent contradictions among the results of different groups, for which the approximations they adopted may be responsible.

Methods and Models.— We solve numerically the equations of neutrino-radiation hydrodynamics. We ap-

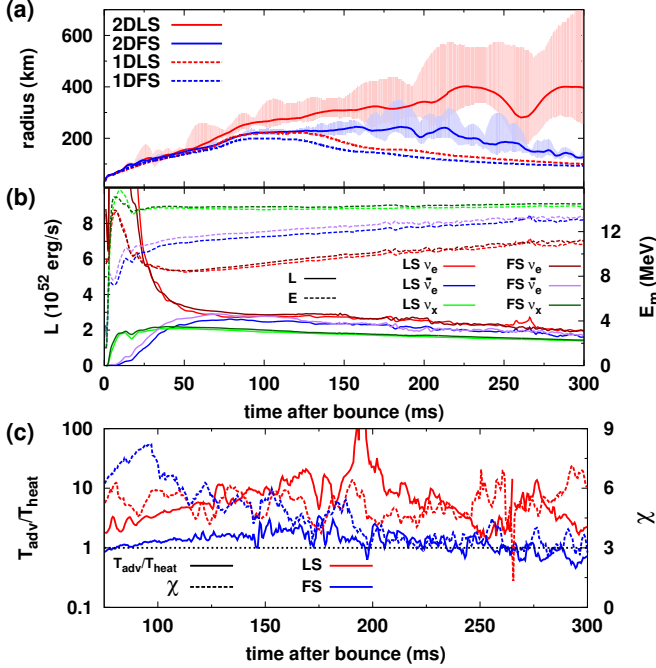


FIG. 1: (a) Shock radii as functions of time. The color-shaded regions show the ranges of the shock radii, red for the LS EOS and blue for the FS EOS. The solid lines are the angle-average values. For comparison, the corresponding results in spherical symmetry are displayed with dashed lines. (b) Time evolutions of the angle-integrated luminosities (L , solid lines) and the angle-averaged mean energies (E_m , dashed lines) for different species of neutrinos. Both of them are measured at $r = 500$ km. (c) The ratio of the advection to heating timescales (T_{adv}/T_{heat} , with solid lines) and the χ parameter (dashed lines). The dotted black line represents $T_{adv}/T_{heat} = 1$ and $\chi = 3$ for reference.

ply the so-called discrete-ordinate method to the Boltzmann equations for neutrino transport, taking fully into account special relativistic effects. In fact, it has already incorporated general relativistic capabilities as well, a part of which is utilized to track the proper motion of proto neutron star (PNS) [34]. The hydrodynamics and self-gravity are still Newtonian: the so-called central scheme of second-order accuracy in both space and time is employed for the former and the Poisson equation is solved for the latter.

We adopt spherical coordinates (r, θ) covering $0 \leq r \leq 5000$ km and $0^\circ \leq \theta \leq 180^\circ$ in the meridian section. We deploy $384(r) \times 128(\theta)$ grid points. Momentum space is also discretized with 20 energy mesh points covering $0 \leq \varepsilon \leq 300$ MeV and $10(\bar{\theta}) \times 6(\bar{\phi})$ angular grid points over the entire solid angle. The polar and azimuthal angles $(\bar{\theta}, \bar{\phi})$ are measured from the radial direction. Three neutrino species are distinguished: electron-type neutrinos ν_e , electron-type anti-neutrinos $\bar{\nu}_e$ and all the others collectively denoted by ν_x .

We pick up a non-rotating progenitor model of $11.2 M_\odot$ from [35]. We employ two nuclear EOS's: Lat-

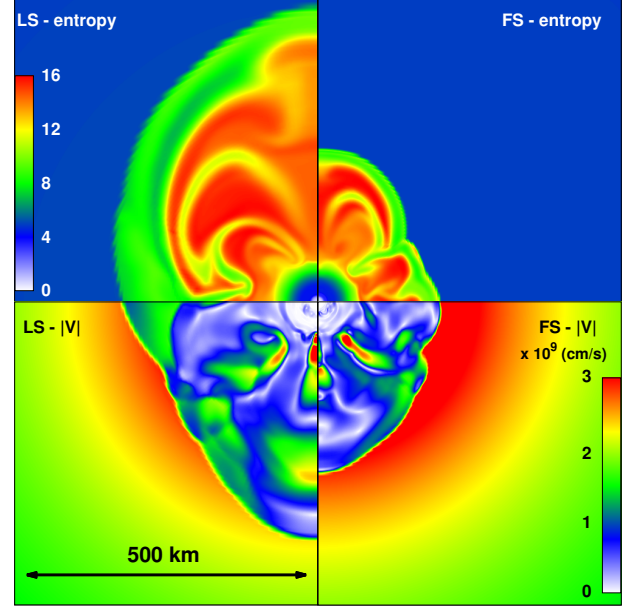


FIG. 2: Snapshots of entropy per baryon (upper) and fluid-speed (lower) at $t = 200$ ms. Left and right panels are for the LS- and FS EOS, respectively.

timer & Swesty's EOS with the incompressibility of $K = 220$ MeV [36] and Furusawa's EOS derived from H.Shen's relativistic mean-field EOS with the TM1 parameter set [37, 38]; the former is softer than the latter. In the following, they are referred to as the "LS" and "FS" EOS's, respectively. Neutrino-matter interactions are based on those given by [39], but we have implemented the up-to-date electron capture rates for heavy nuclei [40–42] and incorporated the non-isoeenergetic scatterings on electrons and positrons as well as the bremsstrahlung in nucleon collisions. We refer readers to [32–34] for more details of our code.

We start the simulations in spherically symmetry and switch them to axisymmetric computations at ~ 1 ms after core bounce when a negative entropy gradient starts to develop behind the shock wave and convection is expected to start. We seed perturbations of 0.1% to radial velocities inside the radius of $r = 50$ km. Each model is run up to $t = 300$ ms after bounce.

Dynamics.— We find an explosion when using the LS EOS. This is the first ever successful shock revival obtained in a multi-D simulation at this level of elaboration in neutrino transport. As displayed in Fig. 1(a), the shock wave produced at core bounce expands rather gradually with time for the LS EOS and its maximum radius reaches ~ 700 km at $t = 300$ ms. Note that the explosion is globally asymmetric as shown in Fig. 2. The pending explosion is apparent from the fact that the shock is still expanding at the end of the simulation and a standard diagnostic also indicates a favorable condition for explosion: the advection timescale ($T_{adv} = M_g/\dot{M}$ with M_g and \dot{M} denoting the mass in the gain region and the mass accretion rate, respectively) is much longer than the

heating timescale ($T_{\text{heat}} = |E_{\text{tot}}|/\dot{Q}_\nu$ with E_{tot} and \dot{Q}_ν being the total energy and the heating rate in the gain region, respectively), which can be seen in Fig. 1(c). The neutrino-driven convection is dominant over the standing accretion shock instability (SASI) in aiding the shock revival, which conforms to the χ parameter [43, 44] being consistently larger than 3 during the entire post-bounce phase (Fig. 1(c)).

Note that the explosion just presented may not be so robust, since it is sensitive to the nuclear EOS. In fact, we do not find shock revival when using the FS EOS, which is somewhat stiffer than the LS EOS (Fig. 1(a)). The shock wave for the FS EOS stalls at $r \sim 200\text{km}$ at $t \sim 100\text{ms}$ and then starts to recede at $t \sim 250\text{ms}$ and shrinks back to $r \sim 100\text{km}$ by $t \sim 300\text{ms}$. Fig. 2 compares the entropy and velocity distributions between the two models at $t = 200\text{ms}$. Interestingly, their post-shock morphologies are quite similar to each other and only the scales are different. In fact, the convection is dominant over SASI also in the FS EOS with the χ parameter being higher than 3 until $\sim 250\text{ms}$ (Fig. 1(c)). As a consequence of this difference in scale that is attributable to the differences in the EOS, no shock revival is obtained for the FS EOS simulation, although the neutrino luminosities (L) and mean energies (E_m , defined as the ratio of energy density to number density) are almost identical between the two cases (Fig. 1(b)). Note that the difference in EOS and other microphysics tends to be more remarkable in multi-D than in spherical symmetry [26, 45]. However, this outcome may be affected by the general relativistic gravity (see [11, 46, 47, 49]), which is still lacking in the current simulations and should be studied further.

ν -Distributions in Momentum Space.—Now we turn our attention to novel features of the neutrino distributions in moment space. They were never accessible to previous simulations, which integrated out the angular degrees of freedom in momentum space. We find in our calculations significant non-axisymmetry with respect to the radial direction in the neutrino angular distributions. It is produced by lateral inhomogeneities in matter, which are generated by hydrodynamical instabilities. The asymmetry hence appears inevitably in multi-D.

Fig. 3(a) shows such an example for the angular distributions of ν_e with an energy of $\varepsilon = 11.1\text{MeV}$. Each surface displays the relative intensity of the distribution function at different propagation directions in the fluid-rest frame. Surfaces of different colors depict the distribution functions at three locations on an arbitrarily chosen radial ray and are normalized by their maximum values. The distributions are almost isotropic at $r = 23\text{km}$ (red surface) while they become forward peaked as radius increases, a fact that is well known. What is really new here, as we mentioned above, is that they are non-axisymmetric with respect to the radial direction, which is more apparent in Fig. 3(b). Note that the feature is robust, occurring irrespective of neutrino energies or species.

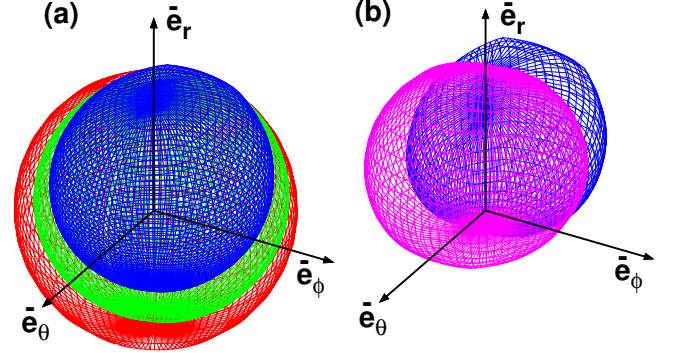


FIG. 3: (a) Angular distributions of ν_e in momentum space at $t_{\text{pb}} = 15\text{ms}$ for the LS EOS. Different colors correspond to different radial positions (red: $r = 23\text{km}$, green: $r = 39\text{km}$, blue: $r = 49\text{km}$) along the radial ray with the zenith angle of $\theta = 96^\circ$. The neutrino energy is $\varepsilon = 11.1\text{MeV}$ in the fluid-rest frame. (b) The deviations from spherical symmetry are emphasized by subtracting the minimum values and re-normalizing the resultant distribution so that the maximum values should be identical in all cases. The blue surface is the same as the one in (a) while the purple surface shows the same wireframe at the same radius of blue one, but at a different zenith angle, $\theta = 68^\circ$.

The multi-angle treatment of neutrino transport in our simulations enables us to evaluate the so-called Eddington tensor (k^{ij}), which characterizes these non-axisymmetric angular distributions more quantitatively. Note that hereinafter Latin subscripts denote the spatial components alone while Greek letters are used for both spatial and temporal components. The Eddington tensor is obtained from the neutrino distribution function (f) as follows: we first define the second angular moment $M^{\mu\nu}$ as

$$M^{\mu\nu}(\varepsilon) = \frac{1}{\varepsilon} \int f(\varepsilon, \Omega_m) p^\mu p^\nu d\Omega_m, \quad (1)$$

where p^μ is the four-momentum of neutrino and ε and Ω_m are the corresponding energy and solid angle measured in the fluid-rest frame; then k^{ij} is given by the ratio P^{ij}/E , where P^{ij} and E are defined from $M^{\mu\nu}$ as

$$P^{ij}(\varepsilon) = \gamma^i_\mu \gamma^j_\nu M^{\mu\nu}(\varepsilon), \quad (2)$$

$$E(\varepsilon) = n_\mu n_\nu M^{\mu\nu}(\varepsilon), \quad (3)$$

with n_μ and γ^i_μ being the unit vector orthogonal to a hypersurface of constant coordinate time and the projection tensor onto this hypersurface, respectively.

We pay particular attention here to one of the off-diagonal components of the Eddington tensor, $k^{r\theta}$. Note that the existence of non-vanishing $k^{r\theta}$ may be an important warning sign that the ray-by-ray(-plus) approxima-

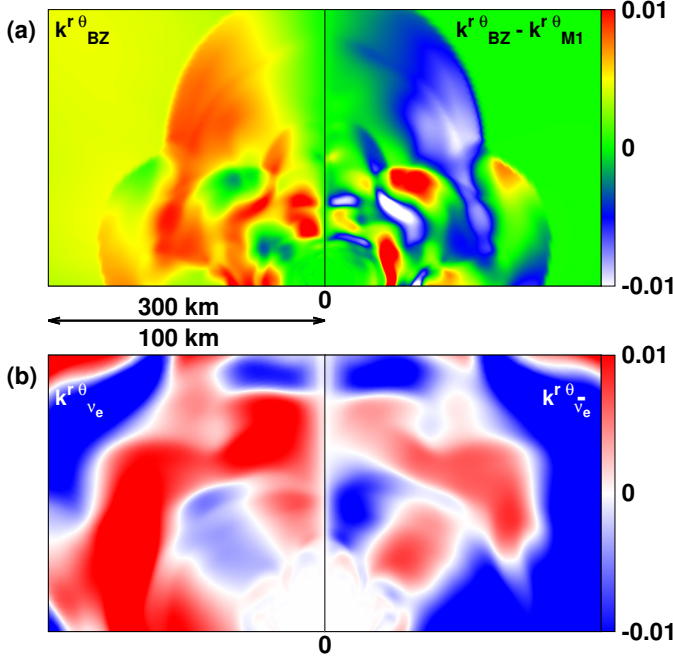


FIG. 4: (a) The $(r\theta)$ component of the Eddington tensor ($k^{r\theta}$) for ν_e in the northern hemisphere obtained in our simulation for the FS EOS (left) and its deviation from the M1 prescription (right). The values of $k^{r\theta}$ are evaluated at the mean neutrino energy at each point. (b) $k^{r\theta}$ for ν_e (left) and $\bar{\nu}_e$ (right) on a smaller spatial scale of 100km. The neutrino energy is fixed to 8.53MeV in the fluid-rest frame. The time is $t = 190\text{ms}$ in all cases.

tion [11–14, 16, 17, 23, 25], which neglects $k^{r\theta}$ completely, may yield inaccurate results.

The left panel in Fig. 4(a) shows $k^{r\theta}$ for ν_e . As expected, it is almost zero inside the PNS, where matter is opaque enough to make the neutrino distribution isotropic. It becomes non-zero outside the PNS, however, and increases with radius in accord with the appearance of the non-axisymmetric structures in the neutrino angular distribution (see Fig. 3). In fact, the $(r\theta)$ component of the Eddington tensor corresponds to the mode with $\ell = 2, m = 1$ in the spherical harmonics expansion of the distribution function.

The right panel in Fig. 4(a) shows, on the other hand, the evidence of a possible problem in the two-moment approximation. This panel compares $k^{r\theta}$ obtained from our simulation with that which is prescribed in the M1 method. The Eddington tensor in the M1 prescription (k_{M1}^{ij}) is obtained by replacing P^{ij} in Eq. (2) with

$$P_{\text{M1}}^{ij}(\varepsilon) = \frac{3\zeta(\varepsilon) - 1}{2} P_{\text{thin}}^{ij}(\varepsilon) + \frac{3(1 - \zeta(\varepsilon))}{2} P_{\text{thick}}^{ij}(\varepsilon), \quad (4)$$

where ζ is referred to as the variable Eddington factor, which we set as $\zeta(\varepsilon) = (3 + 4F(\varepsilon)^2)/(5 + 2\sqrt{4 - 3F(\varepsilon)^2})$ in terms of the so-called flux factor F , which is the flux normalized with the energy density in the fluid-rest

frame. The optically thick and thin limits of P^{ij} are denoted by P_{thick}^{ij} and P_{thin}^{ij} [18, 20, 22, 48]. As clearly seen in this panel, the values of $k^{r\theta}$ are substantially different between the two cases, which is a caution to the M1 approximation. We find that such discrepancies in $k^{r\theta}$ are rather generic, being insensitive to the particular expression of the Eddington factor (see [22] for various options).

Moreover, we find in $k^{r\theta}$ an intriguing correlation/anti-correlation between ν_e and $\bar{\nu}_e$. The two panels of Fig. 4(b) compare $k^{r\theta}$ for ν_e and $\bar{\nu}_e$ with the same energy of $\varepsilon = 8.5\text{MeV}$. As can be seen in these panels, they are anti-correlated with each other in the vicinity of PNS ($\lesssim 50\text{km}$) whereas they are positively correlated at larger radii ($> 80\text{km}$). The anti-correlation is particularly remarkable for low-energy neutrinos with $\lesssim 10\text{MeV}$. We find that the sign of $k^{r\theta}$ roughly coincides with that of the lateral neutrino flux, which flows in the opposite directions for ν_e and $\bar{\nu}_e$. This is due to the Fermi-degeneracy of ν_e at $r \lesssim 30\text{km}$, which produces opposite trends in the number densities of ν_e and $\bar{\nu}_e$. Importantly, the anti-correlation is then carried to larger radii by the outward flux and remains non-vanishing even at $r \sim 50\text{km}$, where ν_e is no longer degenerate. On the other hand, at even larger radii, where matter is optically thin to neutrinos, $k^{r\theta}$ is correlated with the lateral velocity of matter due to relativistic aberration. Note that this positive correlation at large distances is less remarkable than the anti-correlation in the vicinity of PNS (see the equatorial region in Fig. 4(b)), since the angular distribution is no longer determined locally.

Summary and Discussion.—We have reported for the first time a successful shock revival in a multi-D simulation with no artificial approximation except for the mandatory discretization of the differential equations in the Boltzmann-neutrino transport. Although the progenitor we employed in this study produced explosions rather commonly in other approximate simulations and our results share with them the qualitative trend that softer EOS's are advantageous for shock revival, it should be pointed out that the shock propagation after revival seems much less vigorous in our simulation than in others (see e.g., [14]). Detailed analyses are currently underway and will be published elsewhere.

The complicated features in the neutrino distribution in momentum space, such as the lack of axisymmetry and the non-vanishing off-diagonal component of the Eddington tensor, have never been obtained in other approximate simulations done so far. We need to compare our results with those obtained in other approximate simulations quantitatively more in detail. They will provide us with invaluable information that is not only indispensable to understand the origin of the differences we observed in the dynamics of shock revival but will also enable us to calibrate and possibly improve the prescriptions, which should be set by hand in the approximate transport schemes. This is indeed important practically, since our method is very costly in terms of required nu-

merical resources.

There are certainly other issues remaining to be addressed. We are currently implementing general relativity in our code to investigate its influences, which are expected to be non-negligible. Moreover, the angular distributions for different species of neutrinos are valuable in their own right for e.g. the analysis of collective oscillations of neutrino flavors. We are the only ones at present that can provide such realistic data.

Acknowledgments.— H.N. acknowledges to C. D. Ott, S. Richers, L. Roberts, D. Radice, M. Shibata, Y. Sekiguchi, K. Kiuchi and T. Takiwaki for valuable comments and discussions. The numerical computations were performed on the supercomputers at K, at AICS, FX10 at Information Technology Center of Tokyo University, SR16000 at YITP of Kyoto University, and SR16000 and Blue Gene/Q at KEK under the support of its Large Scale Simulation Program (14/15-17, 15/16-08, 16/17-

11), Research Center for Nuclear Physics (RCNP) at Osaka University, the XC30 and the general common use computer system at the Center for the Computational Astrophysics, CfCA, the National Astronomical Observatory of Japan. Large-scale storage of numerical data is supported by JLDG constructed over SINET4 of NII. H.N and S.F were supported in part by JSPS Postdoctoral Fellowships for Research Abroad No. 27-348 and 28-472 and H.N was partially supported at Caltech through NSF award No. TCAN AST-1333520. This work was supported by Grant-in-Aid for the Scientific Research from the Ministry of Education, Culture, Sports, Science and Technology (MEXT), Japan (15K05093, 24103006, 24105008, 24740165, 24244036, 25870099, 26104006, 16H03986) and HPCI Strategic Program of Japanese MEXT and K computer at the RIKEN and Post-K project (Project ID: hpci 140211, 150225, 160071, 160211).

-
- [1] S. V. Bergh and G. A. Tammann, *Ann. Rev. Astron. Astrophys.* **29**, 363 (1991).
 - [2] E. Cappellaro, M. Turatto, Benetti, D. Y. Tsvetkov, O. S. Bartunov and I. N. Makarova, *Astron. Astrophys.* **273**, 383 (1993)
 - [3] G. A. Tammann, W. Loeffler and A. Schroder, *Astrophys. J. Suppl.* **92**, 487 (1994).
 - [4] B. C. Reed, *Astron. J.* **130**, 1652 (2005)
 - [5] R. Diehl *et al.*, *Nature* **439**, 45 (2006)
 - [6] D. Maoz and C. Badenes, *Mon. Not. Roy. Astron. Soc.* **407**, 1314 (2010)
 - [7] W. Li *et al.*, *Mon. Not. Roy. Astron. Soc.* **412**, 1441 (2011)
 - [8] R. M. Bionta *et al.*, *Phys. Rev. Lett.* **58**, 1494 (1987).
 - [9] K. Hirata *et al.* [Kamiokande-II Collaboration], *Phys. Rev. Lett.* **58**, 1490 (1987).
 - [10] C. D. Ott, A. Burrows, L. Dessart and E. Livne, *Astrophys. J.* **685**, 1069 (2008)
 - [11] B. Muller, H. T. Janka and A. Marek, *Astrophys. J.* **756**, 84 (2012)
 - [12] S. W. Bruenn *et al.*, *Astrophys. J.* **767**, L6 (2013)
 - [13] T. Takiwaki, K. Kotake and Y. Suwa, *Astrophys. J.* **786**, 83 (2014)
 - [14] S. W. Bruenn *et al.*, *Astrophys. J.* **818**, no. 2, 123 (2016)
 - [15] J. C. Dolence, A. Burrows and W. Zhang, *Astrophys. J.* **800**, no. 1, 10 (2015)
 - [16] E. J. Lentz *et al.*, *Astrophys. J.* **807**, no. 2, L31 (2015).
 - [17] T. Melson, H. T. Janka and A. Marek, *Astrophys. J.* **801**, no. 2, L24 (2015)
 - [18] T. Kuroda, T. Takiwaki and K. Kotake, *Astrophys. J. Suppl.* **222**, no. 2, 20 (2016)
 - [19] M. A. Skinner, A. Burrows and J. C. Dolence, arXiv:1512.00113 [astro-ph.SR].
 - [20] E. O'Connor and S. Couch, arXiv:1511.07443 [astro-ph.HE].
 - [21] K. C. Pan, M. Liebendorfer, M. Hempel and F. K. Thielemann, *Astrophys. J.* **817**, no. 1, 72 (2016)
 - [22] O. Just, M. Obergaulinger and H. T. Janka, *Mon. Not. Roy. Astron. Soc.* **453**, no. 4, 3386 (2015)
 - [23] A. Summa, F. Hanke, H. T. Janka, T. Melson, A. Marek and B. Muller, *Astrophys. J.* **825**, no. 1, 6 (2016)
 - [24] L. F. Roberts, C. D. Ott, R. Haas, E. P. O'Connor, P. Diener and E. Schnetter, arXiv:1604.07848 [astro-ph.HE].
 - [25] H. Andresen, B. Mueller, E. Mueller and H. T. Janka, arXiv:1607.05199 [astro-ph.HE].
 - [26] A. Burrows, D. Vartanyan, J. C. Dolence, M. A. Skinner and D. Radice, arXiv:1611.05859 [astro-ph.SR].
 - [27] A. Mezzacappa, M. Liebendorfer, O. E. B. Messer, W. R. Hix, F. K. Thielemann and S. W. Bruenn, *Phys. Rev. Lett.* **86**, 1935 (2001)
 - [28] M. Liebendorfer, M. Rampp, H.-T. Janka and A. Mezzacappa, *Astrophys. J.* **620**, 840 (2005)
 - [29] K. Sumiyoshi, S. Yamada, H. Suzuki, H. Shen, S. Chiba and H. Toki, *Astrophys. J.* **629**, 922 (2005)
 - [30] R. Buras, M. Rampp, H.-T. Janka and K. Kifonidis, *Astron. Astrophys.* **447**, 1049 (2006)
 - [31] E. J. Lentz, A. Mezzacappa, O. E. Bronson Messer, M. Liebendorfer, W. R. Hix and S. W. Bruenn, *Astrophys. J.* **747**, 73 (2012)
 - [32] K. Sumiyoshi and S. Yamada, *Astrophys. J. Suppl.* **199**, 17 (2012)
 - [33] H. Nagakura, K. Sumiyoshi and S. Yamada, *Astrophys. J. Suppl.* **214**, no. 2, 16 (2014)
 - [34] H. Nagakura, W. Iwakami, S. Furusawa, K. Sumiyoshi, S. Yamada, H. Matsufuru and A. Imakura, arXiv:1605.00666 [astro-ph.HE].
 - [35] S. E. Woosley, A. Heger and T. A. Weaver, *Rev. Mod. Phys.* **74**, 1015 (2002).
 - [36] J. M. Lattimer and F. D. Swesty, *Nucl. Phys. A* **535**, 331 (1991).
 - [37] S. Furusawa, S. Yamada, K. Sumiyoshi and H. Suzuki, *Astrophys. J.* **738**, 178 (2011)
 - [38] S. Furusawa, K. Sumiyoshi, S. Yamada and H. Suzuki, *Astrophys. J.* **772**, 95 (2013)
 - [39] S. W. Bruenn, *Astrophys. J. Suppl.* **58**, 771 (1985).
 - [40] A. Juodagalvis, K. Langanke, W. R. Hix, G. Martinez-Pinedo and J. M. Sampaio, *Nucl. Phys. A* **848**, 454 (2010)
 - [41] K. Langanke and G. Martinez-Pinedo, *Nucl. Phys. A* **673**, 481 (2000)

- [42] K. Langanke *et al.*, Phys. Rev. Lett. **90**, 241102 (2003)
- [43] T. Foglizzo, L. Scheck and H.-T. Janka, Astrophys. J. **652**, 1436 (2006)
- [44] W. Iwakami, H. Nagakura and S. Yamada, Astrophys. J. **786**, 118 (2014)
- [45] F. Hanke, A. Marek, B. Muller and H. T. Janka, Astrophys. J. **755**, 138 (2012)
- [46] S. M. Couch, Astrophys. J. **765**, 29 (2013)
- [47] Y. Suwa, T. Takiwaki, K. Kotake, T. Fischer, M. Liebendoerfer and K. Sato, Astrophys. J. **764**, 99 (2013)
- [48] M. Shibata, K. Kiuchi, Y. i. Sekiguchi and Y. Suwa, Prog. Theor. Phys. **125**, 1255 (2011)
- [49] E. O'Connor and S. Couch, arXiv:1511.07443 [astro-ph.HE].